EVAPORATION OF AN ACOUSTICALLY LEVITATED DROPLET

B. Zaitone[1], S. Hunsmann[2], G. Castanet[1], N. Damaschke[1], V. Ebert[2] and Tropea[1]

[1] Fachgebiet Stromungslehre und Aerodynamik, Darmstadt University of Technology, Petersenstrase 30, D-64287 Darmstadt, Germany Tel. +49-6151-162854
Email: guillaume.castanet@sla.tu-darmstadt.de

[2] Physikalisch-Chemisches Institut, Heidelberg University, Neuenheimer Feld 253, D-69120 Heidelberg, Germany Tel. +49-62 21-54 5004
Email: volker.ebert@pci.uni-heidelberg.de

ABSTRACT The rate of heat and mass transfer to droplets in sprays is a critical issue in the design of many practical spray systems. Applications like fuel injection in internal combustion engines or spray drying stimulate interest in studying the processes related to the evaporation of droplets. Since experiments on real sprays are difficult to conduct and interpret, simpler and idealized configurations are generally preferred. An acoustic levitator is used to observe a droplet during the entire time of its evaporation. The introduction of a droplet into the sound field leads to the formation of two steady toroidal vortices close to the droplet surface. The results illustrate how this 'outer acoustic streaming' affects the heat and mass transfer. A calibration-free, high-resolution laser absorption spectrometer intended for the non-intrusive detection of the water vapour distribution around the droplet has been developed and used for first experiments. A sensitivity of 1500 ppm in a 1mm absorption path could be demonstrated. The present study is also part of larger project aiming to implement highly resolved measurement techniques to observe the heat and mass transfers in the vicinity of the droplet surface or within the droplet.

Keywords: Acoustic levitation, droplet evaporation, heat and mass transfer, laser absorption spectrometry

1. INTRODUCTION

The improvement of the basic understanding of heat and mass transfer in sprays is a key point in many engineering applications such as spray cooling of hot surfaces, prevention of aircraft icing or in the highly competitive field of fuel injection in internal combustion engines. The entire spray process consists of multiple physical phenomena: primary atomization, spray transport, and wall interactions, as well as single droplet processes, i.e. evaporation and heating during spray transport. The quality of the predictive tools in this field is highly related to the level of physical knowledge of the different elementary phenomena. Simulations are generally based on observation from isolated droplets and assuming spherical symmetry of the transfer at the droplet scale [1,2]. Recent studies on moving droplets have demonstrated the necessity of three dimensional models to take into account the complexity of the aerodynamic field and its consequences on the temperature and vapor distributions. To develop and validate such models, highly resolved measurements are required in the vicinity of the droplet surface. Absorption spectrometry is relatively well-established technique that has demonstrated such capabilities to measure the vapor concentration.

Due to the complexity of the experiments on full scale sprays, simple configurations, such as single droplets, are usually used to obtain basic information. For carrying out such experiments, the droplet can be suspended on the tip of a needle or a thin wire. The reliability and the accuracy of techniques with mechanical suspension suffer from the influence of the needle or the wire, which affects the heat and mass transfer due to heat conduction and droplet surface deformation. Zero-gravity drop towers have also been used for investigating single-drop evaporation; however these are rather complicated facilities. Acoustic levitators are a useful tool to suspend a drop without contact. In principle, the possibility to sustain a certain air flow enables investigation of the effects of convection transport non-intrusively. Nevertheless, despite its advantages as an experimental tool, the levitator introduces some difficulties. One of the main problems is that the acoustic field affects the heat and mass transfer by inducing the so-called 'acoustic streaming', with the presence of two steady toroidal vortices close to the droplet surface (figure 1). Investigations of levitated droplets have been performed by several authors [3,4,5], who have given an extensive overview on acoustic levitation and the effects of the acoustic field on droplet physics.

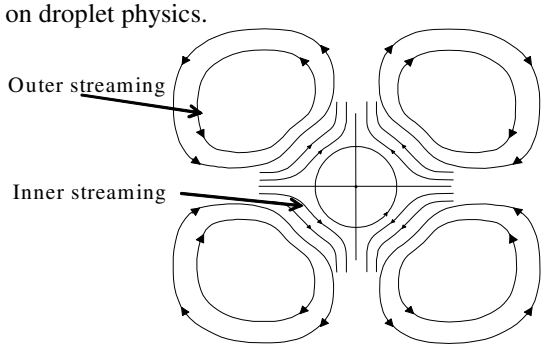

Figure 1 *Sketch of the acoustic streaming field near the levitated droplet.*

The influence of several parameters such as the acoustic radiation pressure, the air flow velocity of droplet ventilation on the rate of heat and mass transfer will be considered in this present work. The first steps of development of a water vapor concentration measurement system will be also described.

2. EXPERIMENTAL TECHNIQUE

2.1 Experimental Setup

The ultrasonic levitator used for the experiments is sketched in figure 2, it consists of the reflector flange with integrated concave reflector and a micrometer screw for the variation of the reflector distance and the transducer flange with integrated ultrasonic transducer, shielding tube and round socket.

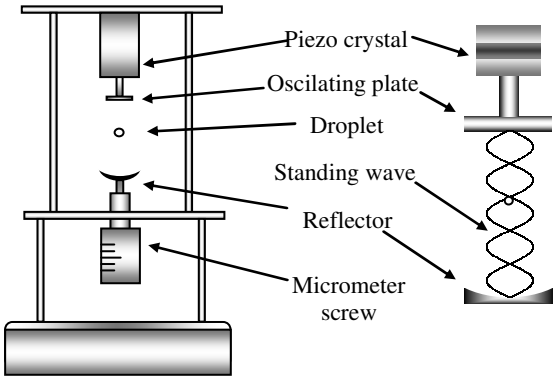

Figure 2 *Schematic picture of acoustic levitator.*

The transducer is connected to an oscillating piezocrystal (f = 58 KHz), transmitting these oscillations to the surrounding air. A standing wave is produced between the transducer and the reflector, the distance between the reflector and the transducer is a multiple of half-wavelengths and was maintained at 1.5 cm which corresponds to 5 pressure nodes in the acoustic levitator. The sound pressure level is then adjusted by changing the driving voltage of the piezocyrstal. The acoustic radiation pressure exerted on a particle produce a vertical force that is strong enough to compensate the gravity. In this case, the particle takes a position slightly below a pressure node. Due to the non-uniformity of the acoustic radiation a liquid sample becomes somewhat oblate. A sketch of the standing wave between the transducer and the reflector is shown in figure 2. Ventilation air enters through an annular grid in the reflector and leaves the levitator at the top through a hole in the transducer. The air is previously dried, so its humidity is never greater than 4%. The reason for ventilation is discussed in more detail in sec. 4. An optional double-walled glass tube allows the connection of a commercial water thermostat. This transforms the chamber into a "miniature climatic chamber".

2.2 Droplet Diameter and Sound Pressure Level Measurements

The droplet is inserted into the acoustic field with a syringe of volume 5µl and with an accuracy of ±0.01 µl. The needle of the syringe can be introduced into the acoustic field via a hole centered in the transducer. Before injecting the droplet into the desired pressure node, the driving voltage is increased in order to overcome the capillary force which attaches the droplet to the needle and helps to stabilize the droplet by damping the oscillations that result from introducing the droplet into the acoustic field. After subsequent adjustment of the sound pressure level at which the experiment is to be started, the droplet is ready for the measurements.

Different liquids were investigated (water and methanol); the initial temperature of the droplets is adjusted to be 22°C, which is also the temperature maintained within the process chamber of the levitator. In order to determine the equivalent drop size, a video system consisting of a CCD camera (800x600 pixels) with a macro lens is used. The magnification factor is determined before the measurements by imaging a high-precision scale etched on a glass plate. The droplet is illuminated from behind using a white light source which enables acquisition of sharp images of the droplet contour. The meridian contour of the droplet is approximated by an ellipse, which has proved to be always a correct approximation even in the presence of low air ventilation. From this oblate shape, the volume of the droplet was calculated assuming axisymmetry. The droplet diameter, vertical position and the aspect ratio are monitored online as a function of time during the droplet evaporation by using an in-house image processing program; the volume equivalent diameter is calculated from the measured major and minor axes S_l and S_s, using the equation:

$$D_{eq} = 2\sqrt[3]{S_l^2 S_s} \tag{1}$$

The heat and mass transfers depends strongly on the sound pressure level (SPL). It is therefore important to know the evolution of the SPL during droplet evaporation. The presence of a large drop decreases the pressure intensity and results in a resonance shift because of the scattering of the acoustic field [4,5]. In principle, the SPL could be measured simply by using a microphone; in this case, a calibration is required. However, in the present study no microphone was used because the acoustic field is easily disturbed by any intrusion.

The SPL is deduced directly from the droplet shape, which results from the equilibrium between the capillary force and the acoustic force. A numerical procedure is described by Yarin *et al*. [5]. It is based on the resolution of the wave equation at the droplet surface and for an arbitrary oblate shape. This method has been applied to determine the SPL during droplet evaporation. Typical results are shown in figure 3 for water and methanol droplets. As expected the SPL increases during the evaporation since the scattering effect becomes less. Due to the higher density of water, a higher SPL is generally required for levitation.

2.3 Absolute Diode Laser Based In situ Detection of Water Vapor

Furthermore, a laser-based high-resolution absorption spectrometer to investigate the water vapor distribution surrounding the droplet has been developed.

Water vapor has a very rich ro-vibrational absorption spectrum (figure 4) reaching from the mid infrared, MIR, for the fundamental vibrational transitions at λ= 6.27, 2.74,

2.66 µm, well into the near infrared, NIR, region via overtone and combination bands e.g. at 1.8 and 1.4µm. Using these strong absorption lines it is possible to detect H_2O vapor with considerable sensitivity and selectivity given a tunable narrow-band light source in the MIR.

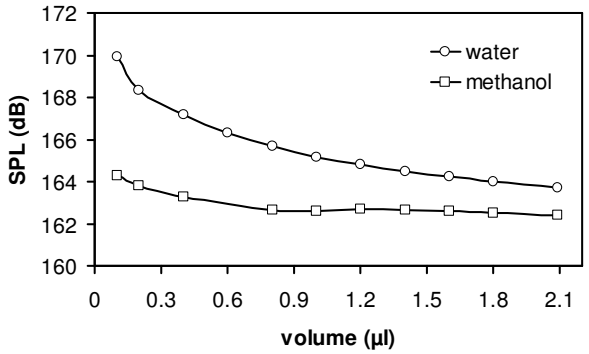

Figure 3 *Computed sound pressure level (SPL) of water droplet during evaporation*

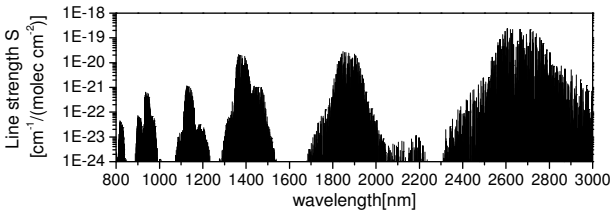

Figure 4 *Ro-vibrational absorption spectrum of water vapor according to HITRAN2004 database[6].*

One of the most versatile and powerful tunable laser sources is the semiconductor diode laser (DL), which has found widespread analytical use. However, to access the stronger MIR bands quite expensive and cumbersome, usually cryogenically cooled DL and detectors have to be used. In contrast, DL for telecommunication and data storage applications, which are available in the 0.63 to 1.65µm region, offer much better technical properties (room temperature operation, high output power, fiber coupling, and room temperature detectors), while still maintaining the excellent spectroscopic features, e.g. high spectral resolution as well as rapid and continuous wavelength tuning, common to all diode lasers. Using such NIR-DL it is possible to exploit the various overtone and combination bands of most polar molecules for analytical purposes. Taking into account the lower band strengths, one can estimate detection limits in the ppm-range (Figure 5), assuming a 1m absorption path and the capability to detect fractional molecular absorption losses $\Delta I/I_0$ of 10^{-4} OD.

Over the last years we developed numerous, sampling-free DL spectrometers for a large number of demanding applications, e.g. simultaneous *in situ* detection of multiple species concentrations and gas temperature in combustion processes [7,8]. The fast, sampling-free detection of water, which is of major interest for the understanding of multiphase flows, has been realized with detection limits of up to 10 ppb and applied to the simultaneous *in situ* H2O/ CH_4-detection in the stratosphere [9] direct sensing of the H_2O super saturation during ice cloud formation and even the simultaneous quantification of water vapor and liquid water mass fraction in dense water sprays [10,11]. This extensive spectroscopic background is currently also employed to investigate the H_2O vapor distribution around a single, acoustically levitated droplet.

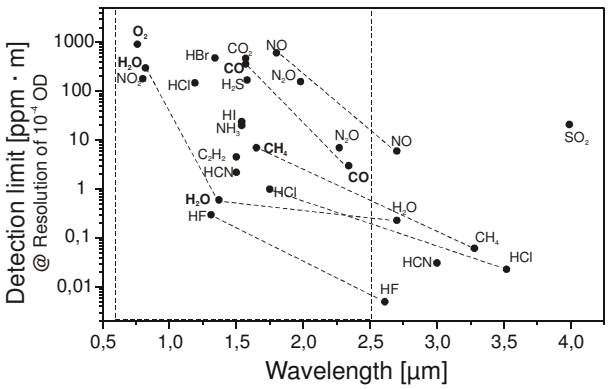

Figure 5 *Species detectable and sensitivities achievable with NIR-DL diode lasers (vibrational overtone transitions of some species connected with dashed lines)*

The basic principle (figure 6) behind these spectrometers is based upon the measurement of the wavelength-specific losses of tunable narrow-band laser light of initial intensity $I_0(\lambda)$ propagating through the measurement volume containing a number density N of absorber molecules as described using the extended Beer's law:

$$I(\lambda,T,t) = I_0(\lambda)\cdot e^{-S(T)\cdot g(\lambda-\lambda_0)\cdot N\cdot z}\cdot Tr(t) + E(t) \qquad (2)$$

Here I(λ, T, t) is the resulting intensity after passage through a probe volume of thickness z. The absorption line is characterized by the temperature dependent line strength S(T) and by the line shape function $g(\lambda-\lambda_0)$ centered at λ_0.

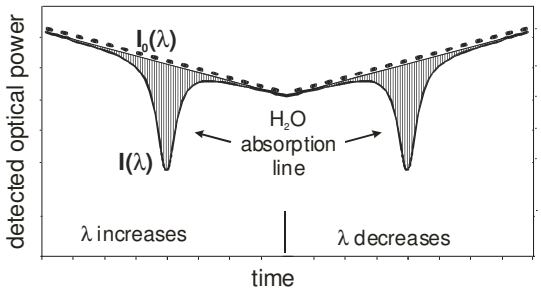

Figure 6 *Basic signal shape of a DL absorption spectrometer*

In situ measurements must contend with two main disturbances [7,8,12]: changes of the transmission Tr(t) of the measurement path, which may be caused by spectrally broadband absorption or scattering (e.g. by particles), and background contributions E(t) to the detector signal due to non-laser light. E(t) may be minimized by narrow-band optical filtering or by exploiting the characteristic amplitude modulation of the laser. Transmission changes are usually more problematic, as they may be larger than the molecular absorption. But since we [7] have developed Tr(t) correction methods that can cope with light losses of up to 99.99% by using the high-speed wavelength tuning capabilities of diode lasers, the minor transmission changes found in a levitator should not be of any problem. Fluctuations in Tr(t) may be eliminated after subtraction of E(t) by a simple division through the reconstructed baseline of the absorption signal; with the 'baseline' being the

detected light intensity, I(λ), in the absence of an absorber. As the laser is scanned without any further modulation and the dc-coupled detector signal is evaluated directly, the method is termed ***direct*** tunable diode laser absorption spectroscopy, dTDLAS. One very important advantage of dTDLAS is the ability to extract absolute absorber number densities without calibration as long as the spectral line data and the experimental parameters (p, T) are known.

These principles have been applied in preliminary studies to quantify the water vapor in the free atmosphere with very short absorption paths, similar to these found in our levitator. The experimental setup used for these initial studies consists mainly of an optical sender (a diode laser including the laser driver electronics), some beam shaping optics and a receiver (photodiode and current preamplifier). As a tunable, narrow-band light source we used a fiber-coupled, single-mode, distributed feedback diode laser, DFB-DL, (NEL) with 20 mW nominal output power. This laser which is thermally tunable over 3.5 nm (figure 7) was operated at 18.5 °C and 36.9 mA, thereby emitting light at 1369.97 nm (7299.43 cm^{-1}) as measured with a high resolution Michelson interferometer.

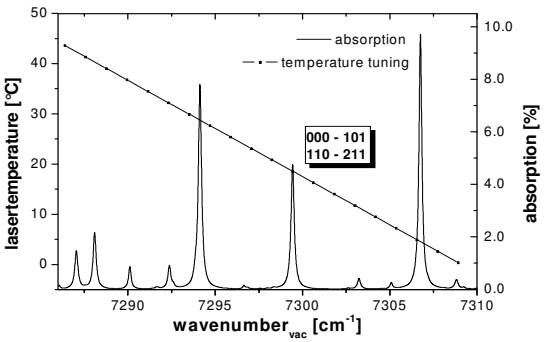

Figure 7 *Temperature tuning of the NIR-DL wavelength and calculated water absorption spectrum assuming 15 cm absorption path in 20% rH room air.*

Applying a 139.8 Hz, 1.7 V_{p-p} triangular waveform from a function generator (SRS) to the diode laser driver (Profile PRO 8000) provided a fast current modulation with 71 mA_{pp} amplitude, which rapidly scanned the laser wavelength across the water vapor 211→110 rotational transition in the 000→101 vibrational combination band (figure 7). This transition was selected with a software based line selection tool due to its high line strength ($9.9x10^{-21}$ cm^{-1}/molecule·cm^{-2} at 296 K) in combination with minimal spectral interference. The laser light exiting the single mode fiber of the laser module will later be collimated by a fiber-to-free-space coupler mounted to the outside wall of the levitator. In our first experiments to determine the optimum sensitivity of our setup we avoided any transmissive optics, which frequently generates significant baseline distortions thus limiting sensitivity and stability [13]. Instead we used a spherical, gold-coated mirror (R=75mm) to focus the beam directly onto the ∅1mm InGaAs photodiode (Epitaxx). The total absorption path from the fiber end to the detector front surface was determined to be 158.1±0.2 mm. The detector output was amplified by a low-noise, variable-gain current amplifier (Femto DLPCA-200), digitized with a 500 kS/s 18 bit DAQ card (NI PCI-6281) and stored on a computer using a custom designed LabVIEW program [7,8]. The individual absorption spectra of 3.57 ms length were digitized with 70 kS/s sample rate. Up to 500 successive scans were averaged to enhance the signal-to-noise ratio, stored to disc and processed off-line by a custom software that identifies the water vapor absorption features, simultaneously compensates for transmission and emission fluctuations, and extracts the area of the absorption line using a Levenberg-Marquart algorithm with approximated Voigt line shapes and background polynomials up to third order. Line areas are converted into H_2O concentrations by applying the extended Beer's Law [7,8], and taking into account the dynamic tuning behavior of the laser [14] well as the measured gas temperature and pressure. It is important to note that this procedure permits the determination of absolute H_2O concentrations without any calibration procedure.

Using this setup we recorded for various boundary conditions the absorption signal of humid room air for the 211→110 transition of water vapor. An unprocessed raw scan and a transmission and emission corrected absorption signal are shown in figure 8 and figure 9.

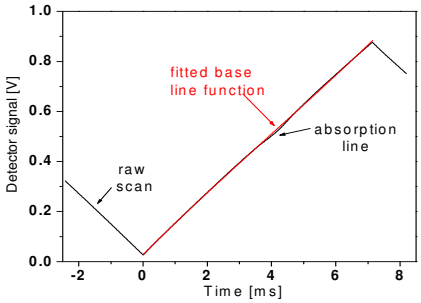

Figure 8 *Raw data from the wavelength scan across the 211→110 transition of water vapor.*

The raw scan is mainly dominated by the very strong, almost linear amplitude modulation, AM, of the laser. AM is an unwanted side effect common to all current tuned diode lasers, which tends to hide the weak molecular absorption signal. To suppress the AM and recover the molecular absorption signal high dynamic range AD-converters and sophisticated data retrieval algorithms are needed. Employing such data treatment and correcting for possible disturbances by transmission or stray light changes, yielded preprocessed data with excellent signal to noise ratios (figure 9). The depicted water absorption signal was gained by averaging 100 consecutive scans within a 1.67s total measurement time. The fitted line shape model shows an excellent match and yields a line width of 0.118 cm^{-1} with a peak absorption of 8%. The residual between fit and model is very small and free of any dominating structure, thus indicating a good suppression of baseline distortions.

The optical resolution as given by the 1σ standard deviation of the residual yields $1.3 \cdot 10^{-4}$ OD which is an excellent value for a dTDLAS setup. This corresponds to a signal to noise ratio of 620:1 or a detection limit of 10 ppm (or 1500ppm with a 1mm absorption path). Further scan averaging may be used to improve the S/N at the expense of measurement speed. The absolute H_2O vapor mixture fraction was determined to be 6448 ± 10 ppm. No calibration was used. Using [15] we calculated the relative humidity, rH, to be 22,51 ± 0.03 % rH.

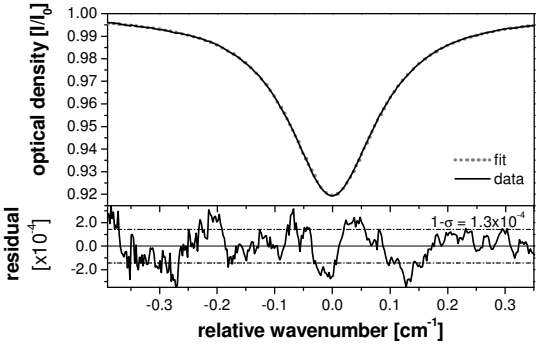

Figure 9 *Processed and fitted absorption signal of the 211→110 transition in room air (100 scan average) as well as the fit residual (bottom).*

In conclusion we have demonstrated a fast, non-intrusive, calibration-free, high resolution humidity sensor based on 1.4µm laser diodes, which has an excellent potential to measure the H_2O vapor distribution around a levitated droplet. From the current performance we already have a sensitivity of 1500 ppm or 5% rH in a 1mm absorption path at a 0.6 Hz measurement bandwidth. This should already be sufficient to provide interesting data for the investigation of transport processes around levitated water droplets. In the future we will employ this sensor to our levitator and simultaneously improve the resolution by use of new 2.6µm diode laser. This should permit sensitivities of 75 ppm or 0.25 % rH in a 1mm absorption path.

3. THEORETICAL DESCRIPTION OF THE MASS AND HEAT TRANSFER MODEL

3.1 Global Approach

A model has been developed to predict the evolution of the size, composition and temperature during the droplet evaporation. Multicomponent droplets are considered and the subscript *i* will be used to designate the ith component of the mixture.

The droplet enthalpy evolution is controlled by the variation of the heat fluxes resulting from forced convection with the surrounding gaseous environment and vaporization. The energy balance can be written as:

$$\Phi_C = \Phi_{vap} + Q_L \tag{3}$$

where Φ_C is the convective heat flux exchanged with the gaseous environment, Q_L is the heat flux entering into the liquid phase and Φ_{vap} is the heat flux due to vaporization defined by:

$$\Phi_{vap} = \sum_i Lv_i \, \dot{m}_i \tag{4}$$

In this expression, the vapor flow rate $\dot{m}_i$ is of positive sign.

The convective heat flux exchanged with the surrounding gas phase at the droplet surface is defined by:

$$\Phi_C = hS\left(T_{amb} - T_S\right) \tag{5}$$

, where *h* is the convective heat transfer coefficient defined by:

$$h = \frac{Nu\lambda_g}{D} \tag{6}$$

S is the droplet surface and T_{amb} is the ambient temperature corresponding to the gas phase temperature surrounding the droplet which characterizes the heat exchanged between the droplet and its environment. *Nu* is Nusselt number, which is defined by:

$$Nu = \frac{D\left.\frac{\partial T_g}{\partial r}\right)_S}{\left(T_{amb} - T_S\right)} \tag{7}$$

Here the Nusselt number is time and space averaged over the period of the acoustic vibration and over the droplet surface.

Since the total vapor flowrate $\dot{m} = \sum \dot{m}_i$, the Nusselt number can be determined using eqs. (3)-(6) :

$$\dot{m} = \pi D \, \rho_g \, a_g B_T Nu \tag{8}$$

where a_g is the gas thermal diffusivity, ρ_g the gas density and B_T is the Spalding heat transfer number defined by:

$$B_T = \frac{Cp_g\left(T_{amb} - T_S\right)}{\sum_i Lv_i \, \beta_i + Q_L \Big/ \dot{m}} \tag{9}$$

In this expression, the parameter β_i is given by:

$$\beta_i = \frac{\dot{m}_i}{\dot{m}} \tag{10}$$

At the droplet surface, the vapor flow rate conservation equation can be written by:

$$\dot{m}_i = \dot{m} Y_{i,S} - \pi D^2 \rho_g D_{i,g} \left.\frac{dY_i}{dr}\right)_S \tag{11}$$

The time and space averaged Sherwood number related to the ith component, defined by:

$$Sh_i = \frac{-D\left.\frac{\partial Yi}{\partial r}\right)_S}{\left(Y_{i,S} - Y_{i,amb}\right)} \tag{12}$$

can be substituted in eq. (11) :

$$\dot{m} = \pi D \rho_g D_{g,i} B_{M,i} Sh_i \tag{13}$$

,where $B_{M,i}$ is the Spalding mass transfer number defined by:

$$B_{M,i} = \left(\frac{Y_{i,S} - Y_{i,amb}}{\beta_i - Y_{i,S}}\right) \tag{14}$$

The comparison between the two expressions, eq. (8) and eq. (13) leads to the following non-dimensional overall energy balance:

$$Le_i \, B_T \, Nu = B_{M,i} Sh_i \tag{15}$$

where Le_i is the Lewis number defined by $Le_i = \frac{a_g}{D_{g,i}}$.

For an acoustically levitated droplet, the heat and mass transfer is driven by the inner acoustic streaming close to the droplet surface. The effect of additional ventilation will be neglected; this assumption will be discussed in the section 4. In the present study, the expressions of the Nusselt and Sherwood numbers are calculated as proposed in [4].

$$Sh_i = K \frac{B}{\sqrt{\omega D_{g,i}}} \tag{16}$$

and

$$Nu = K \frac{B}{\sqrt{\omega a_g}} \tag{17}$$

ω is the angular frequency of the sound vibration, B is a scale of the velocity in the sound wave, defined as:

$$B = \frac{A_{0e}}{\rho_0 c_0} \tag{18}$$

where ρ_0 is the unperturbed air density and c_0 is the sound velocity in air and A_{0e} is the pressure amplitude of the incident sound wave, and related to SPL by:

$$SPL = 20 \log_{10}(A_{0e}) + 74 \tag{19}$$

A_{0e} is in dyne cm^{-2} and the SPL in dB.

K is a dimensionless factor depending, in general, on droplet shape, its displacement from the pressure node, and the sound pressure level SPL. In the case of relatively large drops of 3 µL, K varies in the range of 2–3, while for relatively small drops smaller than 1 µL, K can be approximated by 1.89.

3.2 Calculation Procedure

The temperature, the equivalent diameter of the droplet and the SPL are assumed to be known until the instant t, as well as the ambient conditions (T_{amb}, $Y_{i,,amb}$), which are assumed to be constant. Calculations presented in this section are carried out at each time step separated by the interval δt.

1) The physical properties of the liquid and gaseous phases are calculated. The physical properties of the gas phase are evaluated at the reference state according to the "1/3 rule". The reference conditions are defined by:

$$T_{ref} = T_S + (T_{amb} - T_S)/3 \tag{20}$$

and

$$Y_{i,ref} = Y_{i,S} + (Y_{i,amb} - Y_{i,S})/3 \tag{21}$$

A liquid-vapor equilibrium is assumed in order to determine the vapor fraction $Y_{i,S}$. For ideal gas and liquid mixtures, the molar fraction $X_{i,g}$ in gas phase is related to the molar fraction in the liquid phase $X_{i,l}$ by:

$$X_{i,g} = P_{Si}(T_S) \, X_{i,l} \tag{22}$$

where $P_{Si}(T_S)$ is the vapor saturating pressure of the ith component at the droplet surface temperature T_S.

2) The Sherwood and Nusselt numbers are calculated from eq.(16)and eq. (17). From the Sherwood numbers of each component, the total evaporation flow rate $\dot{m}$ as well as the parameters β_i can be found from eq. (13), knowing that $\sum_i \beta_i = 1$.
3) The non-dimensional overall energy balance eq. (15) is then used to find the heat flux entering into the liquid phase Q_L.
4) Rapid mixing is assumed to determine the new temperature and concentration distribution within the liquid phase. This assumption is justified by the presence of internal motions within the droplet generated by the acoustic streaming in the gaseous phase

4. RESULTS AND DISCUSSION

The influence of ventilation is investigated by blowing dry air over pure water droplets. The temporal evolution of the droplet surface is depicted in figure 10. These results are obtained for droplets evaporated under the same conditions but with different air flow rates, i.e. an initial volume of 2 µL, temperature of 22°C and SPL of 163.7 dB. It can be shown that the droplet surface follows an almost linear evolution with time for any air flow rate, just like for a droplet without any influence of the acoustic field; the diameter regression can be described by the 'D2-Law':

$$(D/D_0)^2 = 1 - K_v \, t \tag{23}$$

where D_0 is the initial droplet diameter and K_v the evaporation rate, i.e. the derivative of the normalized drop surface with respect to time.

It can be also noticed from the results that the droplet evaporation is affected by the ventilation. The sensitivity of the evaporation rate to the blowing is higher for smaller air flows, i.e 0.0 and 0.6 L/min. This effect was not expected since it was known that the evaporation rate of a droplet without acoustic field is normally increased constantly by increasing the air flow rate. This is described by the experimental correlation of Ranz- Marshall [16].

$$K_v / K_{v0} = 2 + 0.6 \, \mathrm{Re}^{1/2} \, \mathrm{Pr}^{1/3} \tag{24}$$

where K_{v0} is the evaporation rate of a motionless droplet without acoustic field.

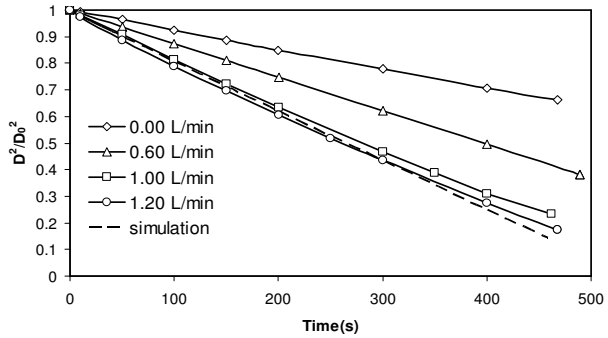

Figure 10 *Normalized surface area vs. time for water droplet evaporation at different ventilation flow rates*

A larger set of experiments were carried out in order to characterize the effect of the blowing more accurately. Air flow rates from 0 to 1.6 l/min were explored, since for larger values, the radial position of the droplet is not stable any more and the droplet may jump out of the node. For all of these measurements, the evaporation rate K_v is determined and its evolution as a function of the ventilation flow rate can be observed in Figure 11. Different domains can be distinguished in the curve.

I. 0-0.4 l/min: almost no variation of the evaporation rate can be seen.
II. 0.4 – 1.0 l/min: the evaporation rate increased significantly.
III. 1 – 1.4 l/min: nearly no effect of blowing can be observed.
IV. 1.4- 1.6 l/min: the evaporation rate starts to increase again with the air flow rate.

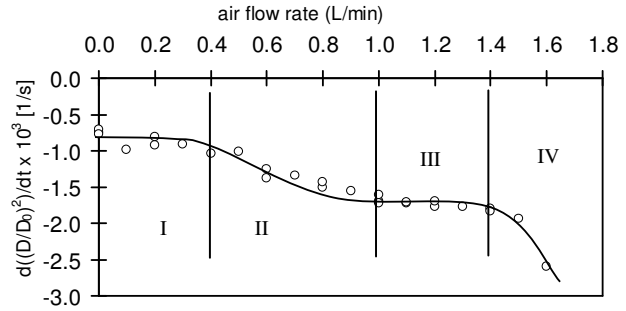

Figure 11 *Evaporation rate versus air flow rate (water droplet of 2µl initial volume).*

The results obtained in figure 11 can be explained by taking into account the influence of the acoustic streaming.
In zone I, the evaporation is reduced due to the vapor enrichment of the droplet neighborhood. The vapor coming from the droplet surface is trapped by the vortices of the outer acoustic streaming (figure 1).
In zone II, the ventilation is enough to deplete the vortices and therefore the evaporation rates increase strongly. The air flow must be greater than 0.4 l/min to influence the surface of the droplet.
In zone III, the depletion of the vortices is completed. The mass transfer is driven only by the inner acoustic streaming that behaves like a 'shield' preventing the air flow to reach the droplet surface.
In zone IV, the ventilation-driven convection begins to play a significant role in the mass transfer.

One can expect that the experimental data obtained in the range of 1-1.4 l/min might be described by the model described in sec. 3, which considers an acoustically-driven mass transfer at constant ambient vapor concentration. This assumption is verified by comparing the simulation results to the experimental surface measurements for different airflows as depicted in figure 10. Good agreement can be noticed for flow rates of 1.0 and 1.2 l/min.
Finally, another liquid is also investigated. The experiment with methanol is carried out for a ventilation of 1.2 l/min, i.e. in the middle of zone III. As shown in figure 12, the experimental results are well predicted by the simulation. This seems to indicate that the position of third zone does not depend really on the evaporated liquid.

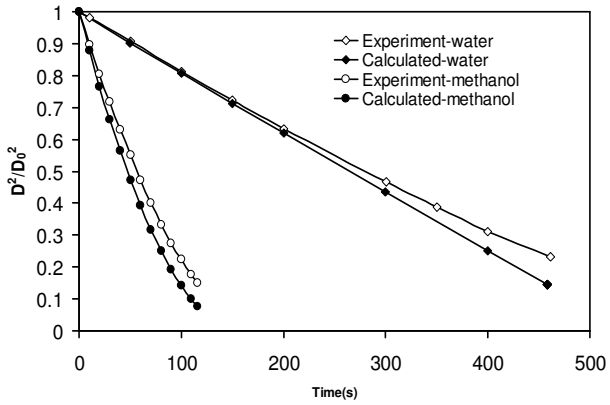

Figure 12 *Temporal evolution of the normalized drop surface for water and methanol droplets with an initial volume of 2µL and initial SPL of 162.3 and 163.7 dB.*

5. CONCLUSION

The evaporation of single acoustically levitated droplets is studied. The measurements of the volume equivalent diameter and axis ratio of the droplets are achieved for two different liquids, methanol and water. The evaporation rate is found experimentally and compared to a theoretical model based on a global quasi-steady approach of the evaporation. A certain ventilation of the droplet is required for a good agreement between the simulations and the experimental data. This result can be explained by the influence of the outer acoustic streaming that is responsible for a vapor enrichment of the droplet neighborhood. In parallel, an experimental set-up has been developed to characterize the vapor concentration field in the vicinity of the droplet surface. A sensitivity of 1500 ppm in a 1mm absorption path could be demonstrated to detect very low vapor concentration. Measurements are expected to reveal the influence of the ventilation on the vapor distribution around a droplet and thus the tri-dimensional effect induced by an external flow on the local mass fluxes.

6. NOMENCLATURE

A_{0e}	Pressure amplitude	[dyne/ cm^2]
a	Thermal diffusivity	[m^2/s]
B_M	Mass transfer Spalding number	[-]
B_T	Thermal transfer Spalding number	[-]
C_p	Specific heat	[J·/kg·K]
c_0	Sound velocity	[m/s]

D	Droplet diameter	[m]
D_g	Molecular diffusivity	[m^2/s]
h	Heat transfer coefficient	[W/K]
K_v	Evaporation rate in acoustic filed	[1/s]
Le	Lewis number	[-]
L_v	Latent heat of vaporization	[J/kg]
$\dot{m}$	Vapor flow rate	[kg/s]
Nu	Nusselt number	[-]
Pr	Prandtl number	[-]
Q_L	Heat flux entering the droplet	[W]
Re	Reynolds number	[-]
S	Droplet surface	[m^2]
Sh	Sherwood number	[-]
S_l	Major Axis	[m]
S_s	Minor Axis	[m]
T	Temperature	[K]
Y	Mass fraction	[-]
X	Molar fraction	[-]

Greek symbols

Φ_C	Convective heat flux	[W]
Φ_{vap}	Vaporization heat flux	[W]
λ	Thermal conductivity	[W/m·K]
μ	Dynamic viscosity	[kg/(m·s)]
ρ	Specific density	[kg/m^3]
ω	Angular frequency of the sound	[rad/s]

Subscripts

Amb	Ambient conditions in the flame
g	Gas phase
l	liquid phase
ref	Reference state

7. REFERENCES

1. Abramzon B., Sirignano W.A., Droplet vaporization model for spray combustion calculations. International Journal of heat and mass transfer, Vol.32, pp.1605, 1989.
2. Sirignano W.A, Fluid dynamics and transport of droplets and sprays, Cambridge University Press, 1999.
3. Trinh E.H., Hsu C.J., Equilibrium shapes of acoustically levitated drops, J. Acoust. Soc. Am., Vol. 79, pp.1335, 1986.
4. Yarin A. L., Brenn G., Kastner O., Rensink D., Tropea C., Evaporation of acoustically levitated droplets, J. Fluid Mech., Vol. 399, pp. 151-204, 1999.
5. Yarin A. L., Pfaffenlehner M., Tropea C., On the acoustic levitation of droplets, J. Fluid Mech.,Vol. 356, pp.65-91, 1998.
6. Rothman L.S. et al., The HITRAN 2004 molecular spectroscopic database, J. Quant. Spectr. & Rad. Transf. 96, 139–204, 2005.
7. Teichert H., Fernholz T., Ebert V., In situ Measurement of CO, H_2O and Gas Temperature in a Lignite-fired Power-plant, Appl. Opt. 42, 2043-2051, 2003.
8. Ebert V., Teichert H., Strauch P., Kolb T., Seifert H., Wolfrum J., High Sensitivity In-situ CO-detection in a 3 MW^{th} Rotary Kiln for Special Waste Incineration Using New 2.3 µm Distributed Feedback Diode Lasers, Proc. Comb. Inst. Vol. 30, 1611-1618, 2005.
9. Gurlit W., Burrows J. P., Zimmermann R., Platt U., Giesemann C., Wolfrum J., Ebert V., Light-Weight Diode Laser Spectrometer "CHILD" for Balloon-borne Measurements of Water Vapor and Methane, Appl. Opt. Vol. 44, 91-102, 2005.
10. Awtry A. R., Fleming J. W., and Ebert V., Simultaneous Diode-Laser-Lased In-situ Measurement of Liquid Water Content and O_2 Mole Fraction in Dense Water Mist Environments, Opt. Lett. Vol. 31, 900-902, 2006.
11. Awtry A. R., Fisher B. T, Moffatt R. A., Ebert V. Fleming J. W., Simultaneous Diode Laser Based Sn situ Quantification of O_2, CO, H_2O Vapor, and Liquid H_2O in a Dense Water Mist Environment, Proc. Comb. Inst. Vol. 31, 2006; accepted.
12. Ebert, V., Fernholz, T., Giesemann, C., Pitz, H., Teichert, H., Wolfrum, J., and Jaritz, H., J. Proc. , Simultaneous Diode-Laser-Based In-situ-Detection of Multiple Species and Temperature in Gas-fired Power-Plants, Comb. Inst. Vol. 28, 423-430, 2000.
13. Ebert V., Teichert H., Giesemann C., Saathoff H., Schurath U., Fiber-coupled in-situ laser absorption spectrometer for the selective detection of water vapor traces down to the ppb-level, Techn. Messen 72, 23-30, 2005.
14. Ebert V., Giesemann C., Koeth J., Teichert H., New Room-Temperature 2.3µm DFB-Diode Lasers: First Spectroscopic Characterization and CO-Detection", in Laser Applications to Chemical and Environmental Analysis, OSA Tech. Digest (Optical Society of America, Washington DC), paper TuF-98, 2004.
15. Buck, A. L., New equations for Computing Vapor Pressure and Enhancement Factor, J. Appl. Meteorol., 20, 1527-1532, 1981.
16. Ranz W.E., Marshall W.R., Evaporation from drops, Chemical engineering progress, Vol. 48, pp.141-180, 1952.